Design Approach of Bolt and Sandwiching Steel Plates in Hybrid-Sandwiching Systems Based on FEM

Alireza Zaferani [a], Pasha Javadi [a,*], Parham Memarzadeh [b]

[a] Department of Civil Engineering, Science and Research Branch, Islamic Azad University, Tehran, Iran.

[b] Department of Civil Engineering, Najafabad Branch, Islamic Azad University, Najafabad, Iran

Abstract

Conventional reduced beam sections (RBS) maintain their capacity with up to 4% drift angle, after which local buckling at the reduced section significantly reduces their resistance. The use of hybrid-sandwiched reduced beam sections (HS-RBS) in the reduced section of conventional RBS beams previously proposed by the authors can increase the energy absorption capacity, allowing the beam to reach 7% drift without losing capacity. The experimental results indicate that placing the HS-RBS in the reduced section of the RBS beam does not disrupt its main role in forming a plastic joint in the reduced section. HS-RBS is comprised of grout, nuts and bolts, and the sandwiching plates. In this system, the bolts and the sandwiching plate enclose the grout and the bolts are placed in the grout on two sides of the beam web in the reduced section to increase the grout's capacity to resist the tensile stresses arising from the web buckling. The sandwiching plate is located in the reduced section on two sides of the flange to enclose the grout and increase the buckling resistance of the flange. This study employed finite element modeling (FEM) to analyze beam bolts with different diameters for different sections of the HS-RBS to obtain the best diameter for each bolt. Moreover, sandwiching plates with different thicknesses were examined to find the best thickness.

1.Introduction

The 1994 Northridge earthquake in the United States and the 1995 Great Hanshin earthquake in Japan inflicted severe damage to the joints of steel structures. Observing the damage in buildings with the moment steel frame indicated that during earthquakes, common moment joints suffer brittle fractures in the weld of the flange to the steel column, leading to poor seismic behavior. Researchers have conducted many studies to find out the reason for the brittle seismic behavior of steel moment frames. One method used to distance the plastic joint from the column to prevent failures in moment frames is to apply reduced beam sections [1].

Plumier [2] first introduced and tested joints with reduced local sections. Popov & Yang [3] introduced RBS sections as a good alternative for transferring plastic joints in the reduced section of beams. The results of Plumier's [4] analysis of stress distribution in the beam-column joint showed beam fracture near the weld, whereas Englehart's [5] test of joints with reduced section showed yield and fracture in the RBS.

Studies by Englehart et al. [6] illustrated that RBS joints with radial cut in the beam flange have sufficient flexibility for meeting the FEMA 351 [7] standard for moment frame joints.

Roeder [8] examined RBS joints and presented the hysteresis diagram of the joint relative to their rotation to illustrate that these joints can ensure good seismic behavior with high plastic rotational capacity. This study presented an equation for achieving the maximum rotational capacity in these joints while introducing the low stiffness outside the web plate as the unfavorable factor in creating the plastic joint in the reduced beam section.

To investigate the type of joint (screw vs. weld) and the resistance of panel zone on the seismic behavior of the moment frame, Lee et al.'s [9] full-scale experiment on RBS joints showed that the welded and bolted joint samples could create adequate flexural capacity based on the criteria of the special moment frame. They also introduced the shear coefficient parameter for the panel zone and found a good

solution for improving the rotational capacity of the plastic joint and reducing the lateral-rotational buckling of the beam in the plastic joint.

To improve the strength and ductility of normal joints, Hedayat & Celikag [10] considered two perpendicular pores on the web of beams, distancing the plastic joint from the end of the beam and the joint to the column. Moreover, the addition of the stiffener in the reduced section of the beam web reduced local buckling in the beam flange and web, thus increasing the ductility of RBS beams.

Lingos et al. [11] evaluated the fragility of joints with RBS. In an experiment, they investigated two main forms of RBS, namely linear and radial. The results suggested that when executed properly, both sections can reach plastic rotation of 3% while maintaining at least 80% of the original capacity. Reducing the flange cross section delays its local buckling but increases the probability of web buckling and lateral rotational buckling due to the flange's reduced stiffness. Mirgaderi et al. [12] introduced a novel type of reduced beam section called accordion web (AW-RBS). This study used the AW-RBS beam in the reduced section of the beam. In AW-RBS, the flat plate of the web is changed to accordion plates (plates folded in L-shape). The experimental results and the finite element model showed that these joints outperform conventional RBS beams with respect to capacity to absorb energy and higher drift of up to 8%. Deylami and Moslehitabar [13] proposed a method for decreasing web buckling in reduced beam sections (RBS) by adding a stiffening plate on both sides of the web in the reduced section of RBS beams. Improving RBS performance, the proposed method has been extensively tested in a large-scale experiment. The results indicated that the proposed RBS connection outperformed conventional RBS under cyclic loading. The proposed sample had 40% greater plastic rotation capacity than conventional RBS connections. Atashbazan et al. [14] compared the behavior of conventional RBS beams to beams with drilled flanges. They deliberately formed a weak zone for non-linear deformations by creating a series of holes on the upper and lower flanges. This study aimed to enhance the performance of RBS connections as a good substitute to conventional RBS connections. The results suggest that these connections provide greater absorption of energy and drift than conventional RBS beams. Morshedi & Maleki [15] introduced a novel steel connection with reduced section and evaluated its seismic performance by using finite element modeling. These connections are formed by two radially-reduced sections in the flange

near the column to achieve a wider plastic joint than conventional RBS beams. Therefore, the plastic strain is equally distributed among the two RBSs. Sheen & Kim [16] considered the most important factor in the seismic performance of beam-column connections in moment steel frames. Both methods RWS (Reduced Web Section) and RBS aim to remove stress from beam-column connections. In this study, they analyzed the RWS approach, which creates a large opening in the web to create plastic mechanism states. The variables in this study included the shape and quantity of openings. Moghaddam and Fanaei [17] evaluated the connection of steel beams to concrete-filled tube (CFT) columns with external T-shaped stiffeners. They analyzed various aspects of perforation, *e.g.*, quantity, diameter, and distance. The results illustrated that perforating the beam flange reduced stress concentration in the beam-column connection, improved beam ductility, and made brittle failure less likely. According to Davarpanah et al. [18], a disadvantage of beam-RBS connections is the possibility of lateral buckling in the reduced section of the beam. Previous studies suggest that reducing the web section instead of the flange is an effective way to prevent lateral buckling. The authors created an oval opening in the beam web near the beam-column connection and provided new details about RWS connections. The results indicated that RWS beams had better resistance, stiffness, ductility, and torsional stability than RBS beams. Nazaralizadeh and Ronagh [19] analyzed the behavior of vertical-slits reduced beam sections (VS-RBS). Multiple perpendicular ovals reduced the web section of these beams. According to this study, the main problem of RBS beams is torsional buckling and reduced flexural strength. The results indicate that VS-RBS beams outperform RBS beams in torsional buckling, flexural strength, and energy loss. This study also compared the PEEQ index, rupture, and energy loss in various samples with different oval dimensions. Chenyu Liu & Jing Wu [20] proposed a new beam connection with a reduced cross-section called buckling restrained RBS (BR-RBS). These connections include buckling restrainer plates at the reduced section of RBS beams. These steel plates can reduce local buckling at the flange and web of the reduced section of RBS, thereby improving the seismic performance of RBS beams. In a laboratory analysis, Chen Liu and Zheng Wu compared RBS sections with the proposed BR–RBS connection. According to their results, restraining lateral buckling in the reduced section of the beam increased energy loss capacity. It can also limit local buckling in the

RBS zone. The results showed greater connection stiffness with BR-RBS than with conventional RBS. These connections exhibited great ductility and withstood up to 0.6% drift angle. Dan V. Bompa and Y. Elghazouli [21] analyzed the behavior of RBS beams by using finite element modeling. This analysis of various sections of RBS beams analyzed the nonlinear behavior and strains developed in various parts of the RBS beam. Two RBS beams with normal section sizes and two thick flange and web were modeled in the software. The results indicated that higher flange thickness in RBS beams prevented local buckling in the reduced section of the beam. This study presented the plastic strain in various reduced sections. V. Sabri and H. Sabri [22] analyzed the behavior of RBS connections by using vertical and horizontal stiffeners in the reduced section. These stiffeners are modeled by ST37 and ST52 steel materials. The results of this study, which employed finite element modeling, showed that the use of two vertical stiffeners and two horizontal stiffeners in the reduced section of the beam increased the initial resistance by 6% and the final resistance by 20% compared with conventional RBS beams. Zaferani et al. [23] proposed a novel method for RBS beams called HS-RBS, where the RBS section is confined by grout, bolts and steel plates. The HS–RBS system incorporated grout in the reduced section of the beam and steel belts around the reduced flange while using bolts to confine the grout. These connections can be rotated to avoid any problems in the flexural performance of the reduced section of RBS beams. Moreover, the proposed system does not change the connection stiffness. Two connections, namely RBS and HS-RBS beams connected to column, were analyzed in the laboratory. One sample was created by using a novel method, and the other was the

conventional RBS. In addition to the laboratory analysis, the components were also analyzed through the FEM, and the results were compared. The results suggest that the use of HS-RBS beams increased the ductility of RBS beams. This design was mainly aimed at preventing local buckling at the reduced section of RBS beams. This study verified steel plates and bolts in the HS-RBS system. Different bolt sizes and steel belts were analyzed for the HS–RBS system. The proposed approach delays the initiation of strength reduction of the end beams' plastic hinges to the 5% drift angle, despite the seismic behavior of commonly detailed RBSs. The bolts and steel belts are responsible for confining the grout in the HS–RBS system. In the event of buckling in the reduced section of the HS–RBS system, the pressure due to local buckling creates tensile stress in the grout, causing deep cracks. The bolts and the belts confine the grout, increasing its strength against tensile stress. In this study, the bolts and the belts were modeled through the FEM Furthermore, the Von-Mises stress of the bolts and the belt caused by buckling in the reduced section of the RBS beam were obtained.

2. Background of the Proposed Hybrid Sandwiching System

2.1. Configuration of Hybrid Sandwiching System

Zaferani et al. [23] proposed a novel method for improving the performance of RBS beams in large drifts. The literature suggests that RBS beams typically remain stable at up to 4% drift angle before suffering a drop in strength and the M–Ө diagram due to local flange and web buckling in the reduced section.
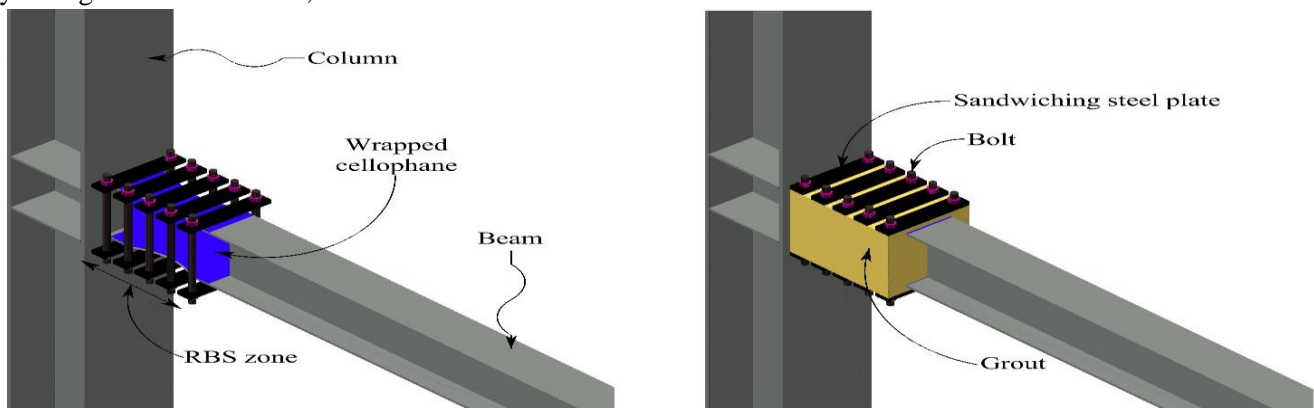

Fig 1. The HS–RBS System in the Reduced Section of the Beam [23]

As shown in Fig.1, The proposed HS–RBS system encloses the reduced section of RBS beams and prevents local buckling in the reduced section of the web and flange. The grout covering the reduced section of the beam, the steel belts on the grout placed on both sides of the reduced flange, and the bolts on both sides of the web inside the grout create lateral confinement. The implementation of discrete steel belts provides rotational freedom in the reduced section of the RBS beam, preventing the HS–RBS components from contributing to the beam's flexural strength. Therefore, like RBS beams, plastic joints will form in the reduced section.

2.2. Brief Review on Experimental Result

The study reviewed by [23] analyzed two specimens of RBS and HS–RBS beams. A beam with an IPE300 section connected to a column with an IPB300 section was used for both specimens. Figure 2 shows the stages of creating an HS–RBS system.
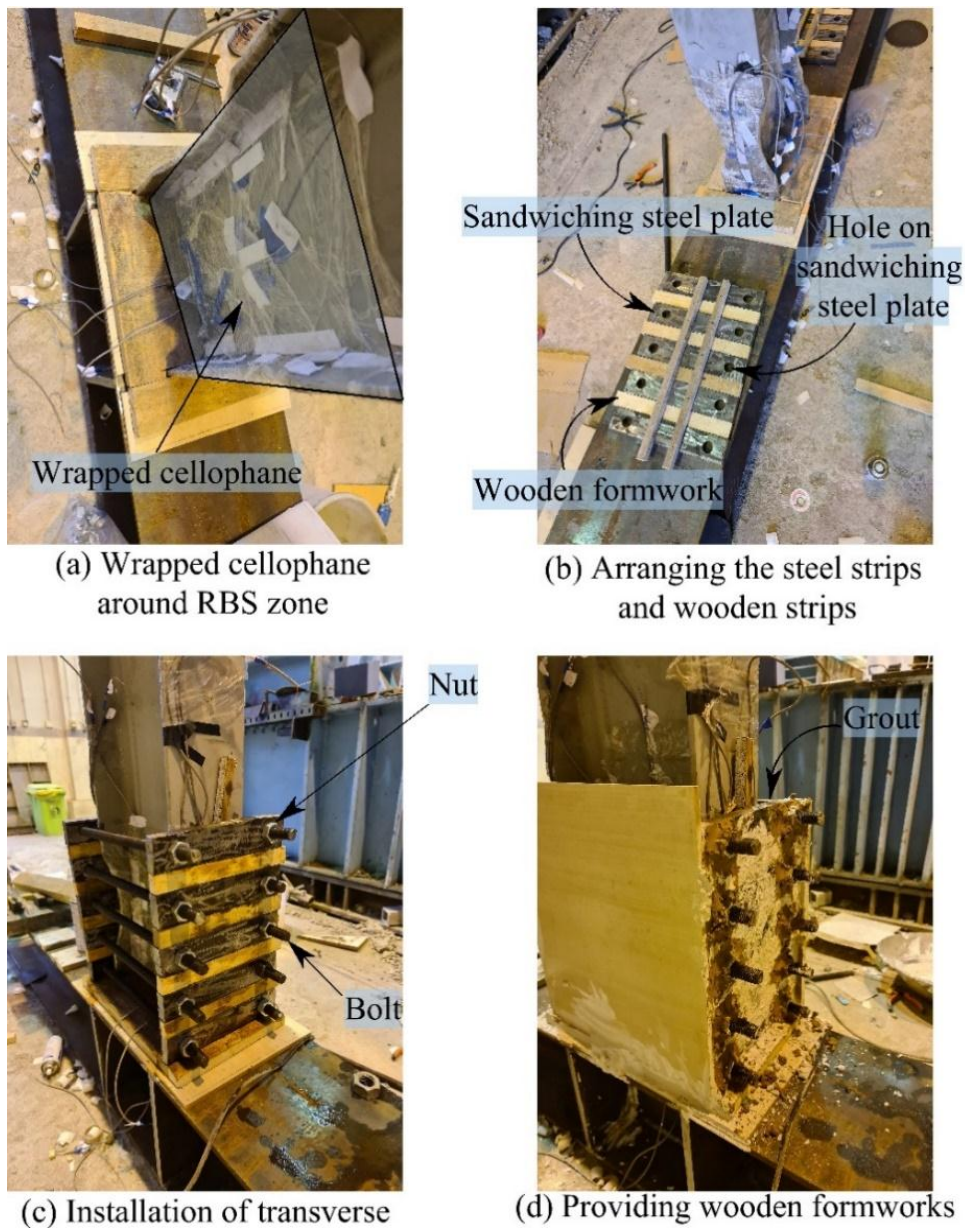

Fig 2. Formwork Stages for HS-RBS [23]

According to Figure 2-(a), to prevent direct contact of the grout to the reduced section of the beam, this section is first fully covered with cellophane to reduce grout adhesion to the flange and web surface of the RBS beam. Eliminating grout adhesion from the column intersection, and all seams are filled with grout. According to Figure 2-(b), steel belts with 5 cm width are placed on the top and bottom of the beam 2.5 cm from the flange. A wooden strips with a width of 3 cm is then placed between each belt. To prevent grout adhesion to the beam and the steel belts, the surfaces of all molds, belts, and even the cellophane are greased. According to Figure 2-(c), the belts on both sides of the beam are connected using bolts with

reduced section of the beam prevents the enclosed section from contributing to the flexural strength of the beam. For formwork in the reduced section of the beam, wooden boards with 3 cm thickness are first placed between the steel belts in the RBS beam– 50 cm length and 20 mm diameter. According to Figure 2-(d), two wooden formworks are placed on the two open sides of the beam web, and all the seams between formworks are filled. The grout was poured from the open section at the top of formwork. According to Figure 3, the HS–RBS model was assembled in the laboratory and was subjected to the AISC360 loading protocol.

Fig 3.The HS–RBS assembly in the Lab [23]

As shown in Fig.4, The results of the moment-drift angle curve of the conventional RBS specimen showed increasing resistance and energy absorption up to drift angle 4%. the hysteresis curve of this specimen deteriorated at first cycle of 5% drift and suffers strength loss. the sample lost its resistance and failed at second cycle of 5%. The results of the moment- drift angle curve in Figure 4 shows that the HS–RBS specimen has rising energy absorption at up to 6% drift. In the first cycle of 7% drift, the hysteresis curve suffers a resistance drop, and in the second cycle, the sample lost its strength.
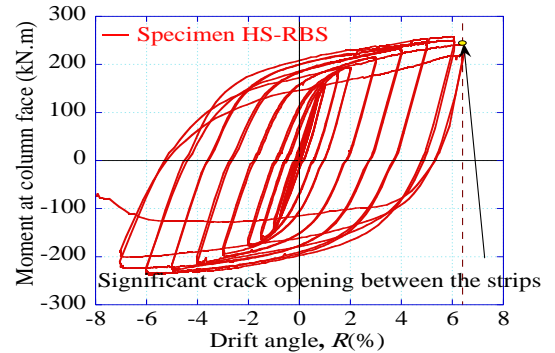

(a) photo of specimen RBS

(b) photo of specimen HS-RBS
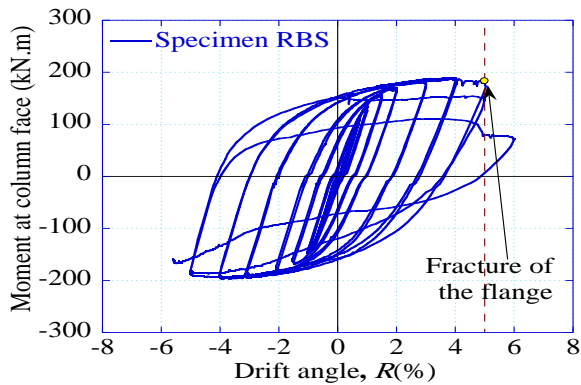
(c) Hysteresis curve of specimen RBS

(d) Hysteresis curve of specimen HS-RBS

Fig 4. The photos and Hysteresis Curves of the specimens [23]

3. Designs of Anchor and Steel Plate

3.1. Considered Failure Mechanisms

In the specimen HS–RBS, the bolts are responsible for confining the grout. In this system, the bolts are placed in the grout on two sides of the web to prevent grout destruction while transferring the pressure caused by web buckling (see Figure 5-(a)). According to Figure 5-(b), the pressure caused by web buckling in the reduced section created flexural cracking in the grout. Web buckling in the reduced section is the cause of tensile stress in the grout. Placing bolts on two sides of the beam web increases the grout resistance to tensile stresses. Figure 5-(c) shows the deformation of bolts caused by web buckling pressure. In this system, the steel plates are also placed on two sides of the reduced flange side of the flange to prevent grout destruction when transferring the pressure caused by flange buckling in the reduced section of the beam. Figure 5-(d) shows the

distribution of the pressure caused by beam flange buckling on the steel plates. According to Figure 5-(e), the pressure caused by flange buckling in the reduced section created flexural cracking in the grout.

Placing these steel sheets on two sides of the beam web increased the grout resistance to tensile stress. Figure 5-(f) shows the deformation of steel plates caused by the pressure of beam flange buckling.
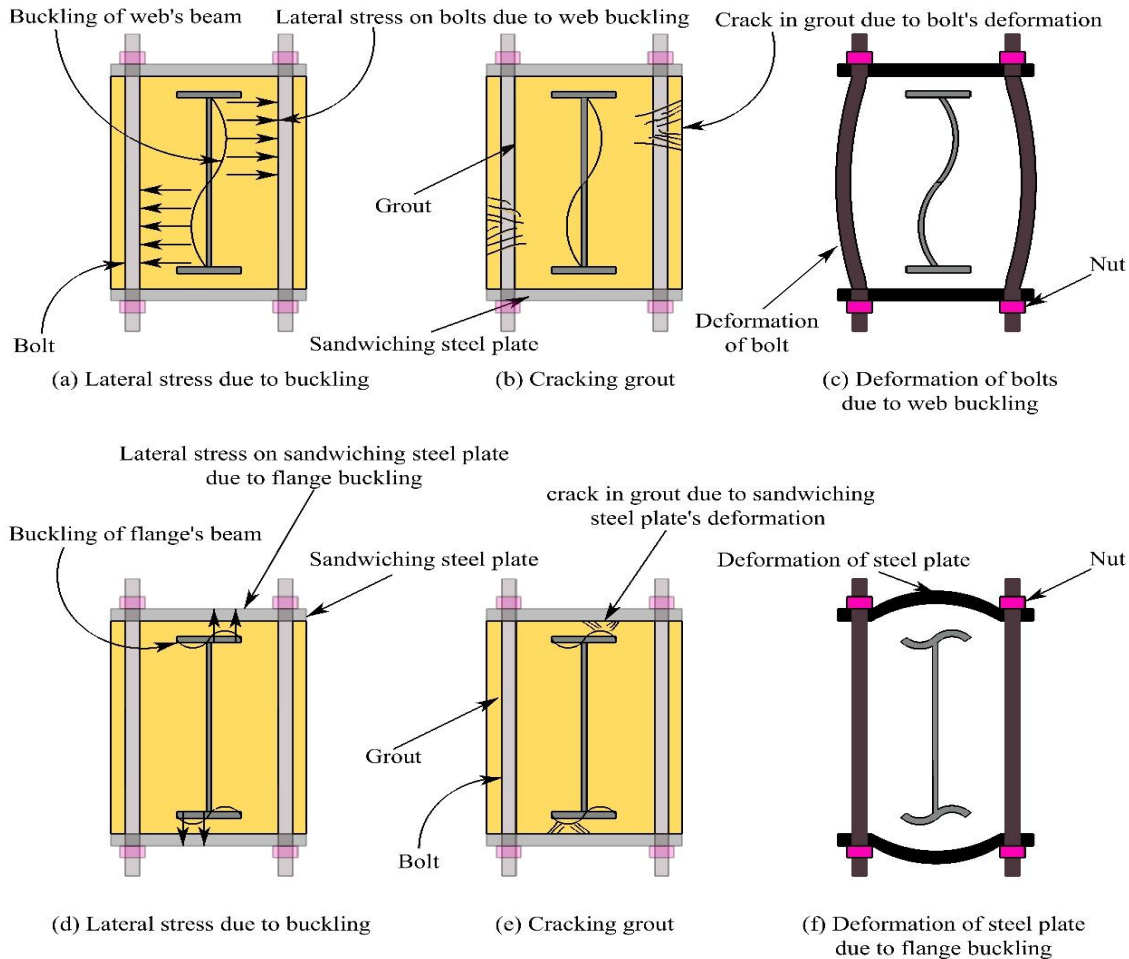

(a) Lateral stress due to buckling

(b) Cracking grout

(c) Deformation of bolts due to web buckling

(d) Lateral stress due to buckling

(e) Cracking grout

(f) Deformation of steel plate due to flange buckling

Fig 5. The Deformation of Bolts and Steel Plates Due to Web and Flange Buckling in the Reduced Section

3.2. Proposed Design Approach for Bolt and Steel Plate

For each section of the beam, one steel plate with half the height and same thickness as the web was modeled in finite element software. Longitudinally, axial displacement was applied to the modeled plate to cause out-of-plane buckling. According to Figure 6-(a), the element at the reduced section of the RBS beam was selected for maximum strain along the beam longitudinal axis. Then, the element hysteresis curve was drawn and shown in Figure 6-(b). Regarding to the strain-displacement curve, the maximum compression strain occurred along the

longitudinal axis of the beam was obtained. According to Figure 6-(c), a plate at the reduced section with half of the web height was modeled in the software. Based on to Figure 6-(d), two rigid plates were placed at two sides of the plate modeled for the web and the support, and displacement boundary conditions applied to the plate were specified These plate play a role as buckling restrained element for simplify the grout and bolts effects. Figure 6-(e) shows the longitudinal strain curve of the plate against the axial displacement in the most critical element of the plate that suffers out-of-plane buckling. According to Figure 6-(f), in the next

stage, the maximum out-of-plane stress in the most critical zone where the plate suffers out-of-plane buckling was determined based on the strain displacement obtained from the previous stage. Regarding to Figure 6-(g), this stress was equal to the pressure applied to half the height of bolts. Then, the deformation and Von Mises stress caused by applying this stress to the bolts was calculated. This process was also repeated for bolts with various sections to determine the best bolt dimensions for each section of the beam. To design the sandwiching plate, the most critical element of the reduced flange section was first selected in accordance with Figure 7-(a). Figure 7-(b) shows the strain hysteresis curve along the longitudinal axis of the flange to determine the maximum strain along the longitudinal axis of the flange. According to 7-(c), a plate was modeled in the software for each section of the beam according to the flange dimensions in the reduced section and with identical thickness. Figure 7-(d) illustrates the support

conditions and the displacement applied to the plate. Then, rigid plates were placed on two sides of the modeled plate. The axial displacement applied to the plate creates out-of-plane buckling in the reduced section. Figure 7-(e) shows this longitudinal strain curve of the plate against the displacement applied to the plate. According to Figure 7-(f), the out-of-plane stress in the most critical zone of the plate to suffer out-of-plane buckling was determined based on the strain displacement obtained from the previous stage. This stress is equal to the pressure applied to the loading surface of the sandwiching plate. Then, according to Figure 7-(g), this stress is applied to half the section of the sandwiching plate. Then, the deformation and Von Mises stress caused by applying this stress to the steel plate was calculated. Steel plates with thicknesses of 10 and 20 mm were then modeled to determine the best plate dimensions for each section of the beam.

Fig 6. The Bolt Design

(a) Compression zone in flange's of RBS

(b) Maximum strain in section B-B

(c) Dimensions of plate model

(d) Confinement and displacement of plate model

(e) Strain along the lenghth of the plate

(f) Out of plate stress of the plate

(g) Applied stress to the sandwiching steel strip
(procedre constines in Fig. 17)
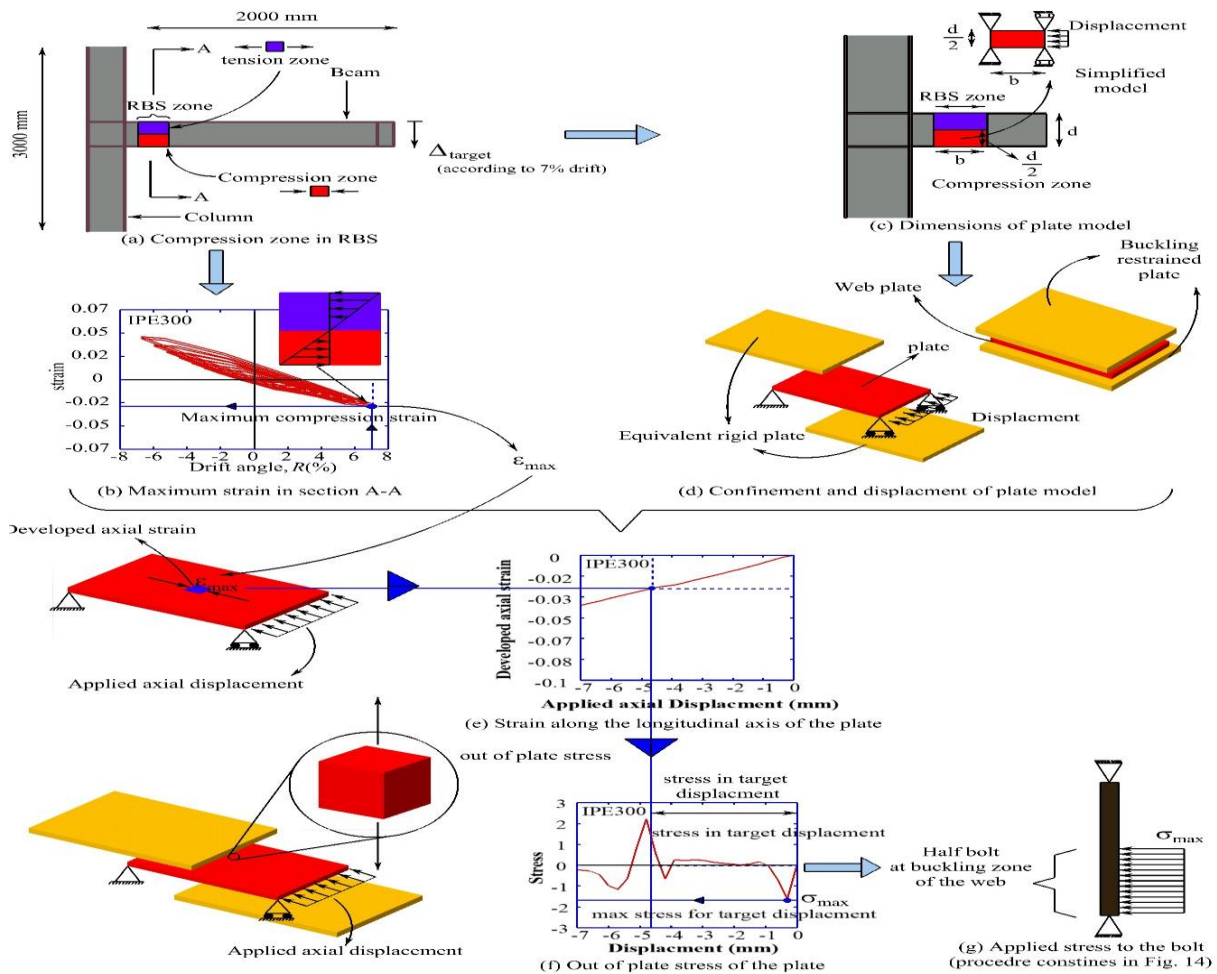
Fig 7. The Sandwiching Plate Design

```
┌─────────────────────────────────────────────────────────────────────────────┐
│  ┌─────────────────────────────────┐      ┌─────────────────────────────────┐ │
│  │   Applying Displacement to      │      │   Applying Displacement to      │ │
│  │   the End of the Beam           │      │   the End of the Beam           │ │
│  │   According to the Target Drift │      │   According to the Target Drift │ │
│  │   (Δtarget)                     │      │   (Δtarget)                     │ │
│  └─────────────────────────────────┘      └─────────────────────────────────┘ │
│                 ↓                                        ↓                      │
│  ┌─────────────────────────────────┐      ┌─────────────────────────────────┐ │
│  │   Maximum Pressure Stain in the │      │   Maximum Pressure Stain in the │ │
│  │   Reduced Section of the Beam   │      │   Reduced Section of the Beam   │ │
│  │   Flange                        │      │   Web                           │ │
│  │   Єmax                          │      │   Єmax                          │ │
│  └─────────────────────────────────┘      └─────────────────────────────────┘ │
│                 ↓                                        ↓                      │
│  ┌─────────────────────────────────┐      ┌─────────────────────────────────┐ │
│  │   Obtaining the Displacement of │      │   Obtaining the Displacement of │ │
│  │   Plates According to the Max.  │      │   Plates According to the Max.  │ │
│  │   Pressure Strain               │      │   Pressure Strain               │ │
│  │   Δ                             │      │   δ                             │ │
│  └─────────────────────────────────┘      └─────────────────────────────────┘ │
│                 ↓                                        ↓                      │
│  ┌─────────────────────────────────┐      ┌─────────────────────────────────┐ │
│  │   Obtaining Maximum Strain σ in │      │   Obtaining Maximum Strain σ in │ │
│  │   the Plate Based on            │      │   the Plate Based on            │ │
│  │   Displacement δ                │      │   Displacement δ                │ │
│  └─────────────────────────────────┘      └─────────────────────────────────┘ │
│                 ↓                                        ↓                      │
│  ┌─────────────────────────────────┐      ┌─────────────────────────────────┐ │
│  │   Applying Maximum              │      │   Applying Maximum Stress to the│ │
│  │   Stress to the Sandwiching     │      │   Bolt                          │ │
│  │   Plate                         │      │                                 │ │
│  └─────────────────────────────────┘      └─────────────────────────────────┘ │
│                                                                                │
│       (A) Sandwiching Plate Modeling              (B) Bolt Modeling            │
└─────────────────────────────────────────────────────────────────────────────┘
```
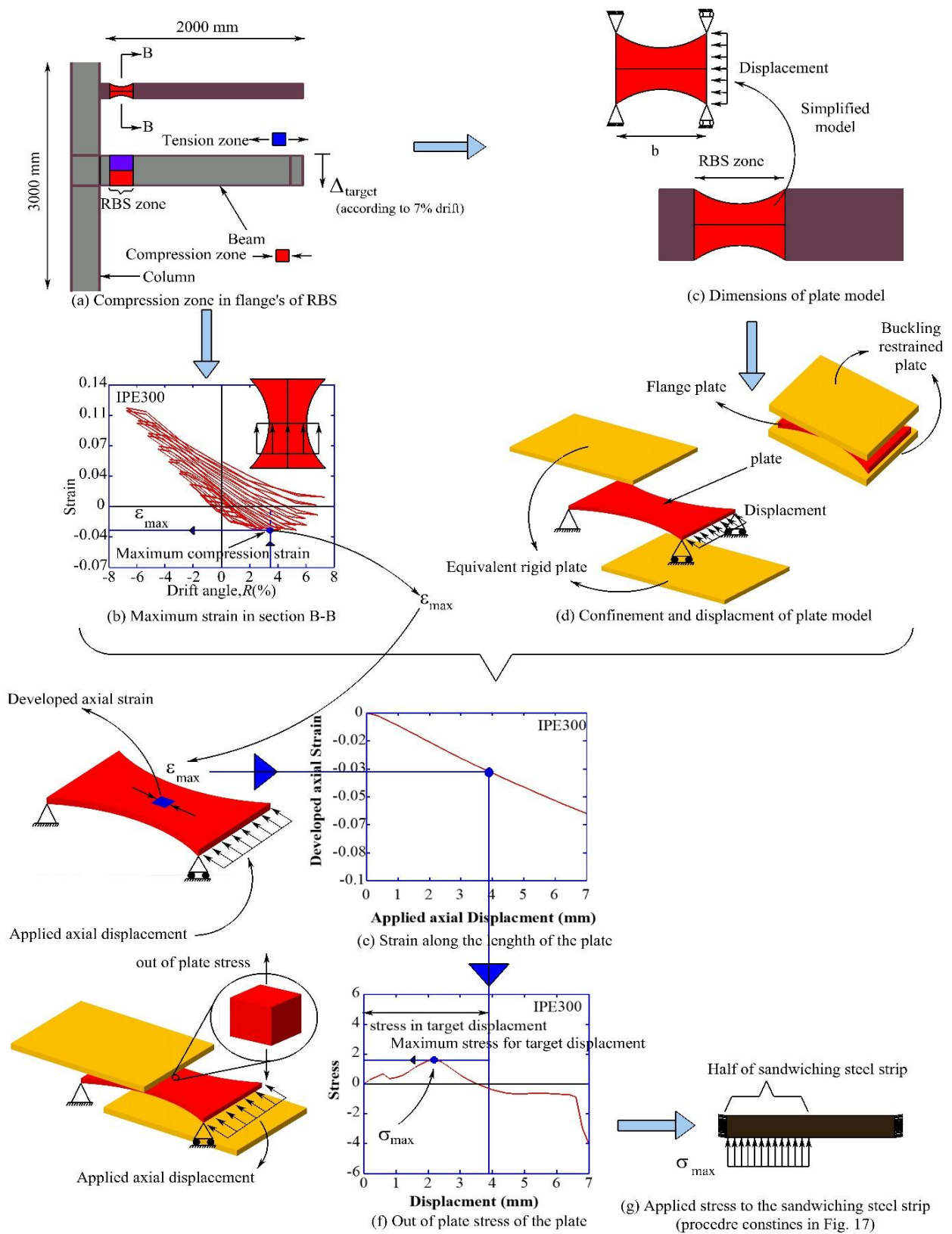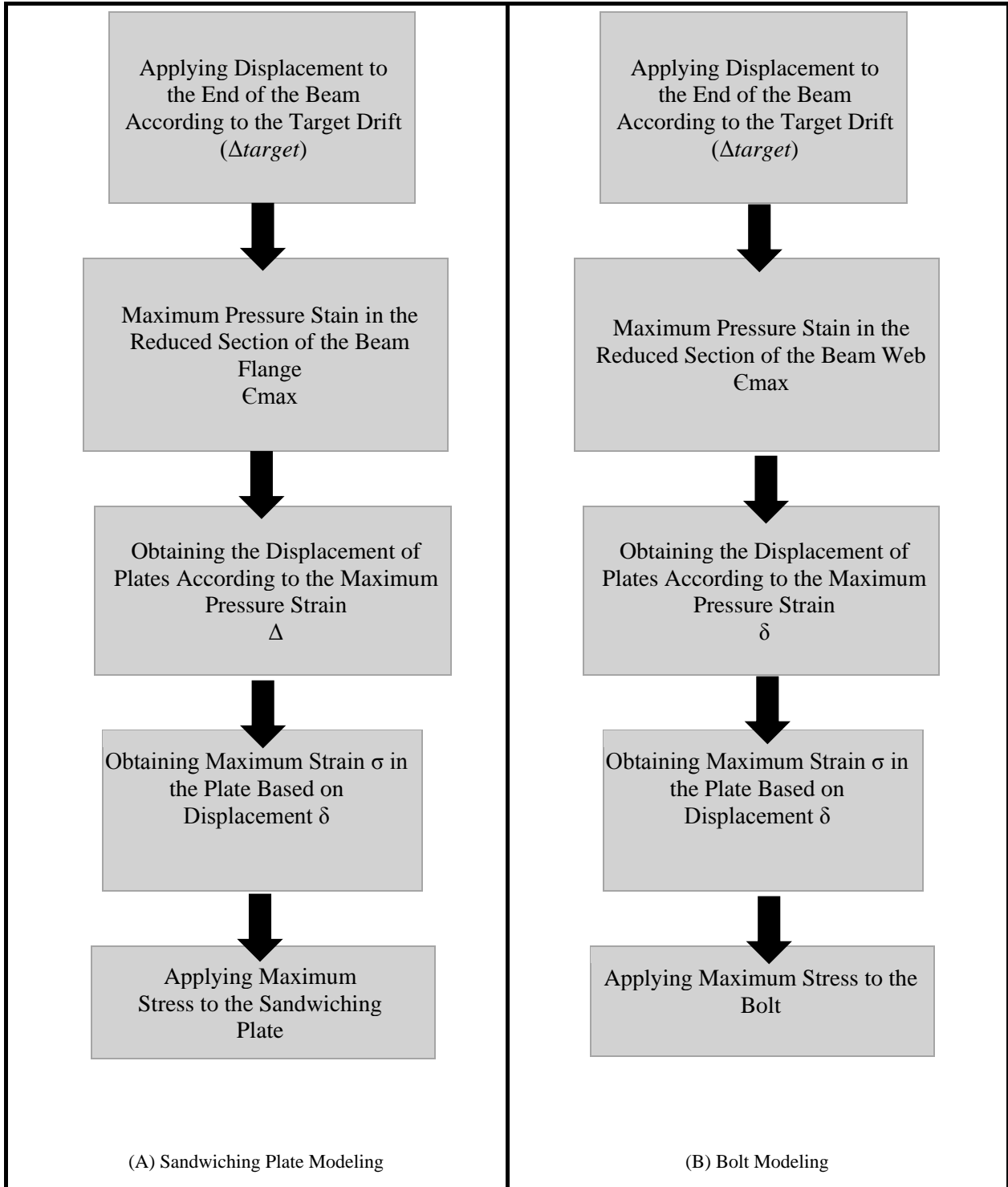
Fig 8. Designing the Bolts and the Sandwiching Plate

Based on to Figure 9-(a), the load width was defined for each section of the beam in accordance with the distance of bolts. Since the loading height under buckling of the web is half of the height of the beam web, the stress applied to the bolts is equal to half of the height of the beam web. Moreover, the load width is equal to the distance of bolts. According to Figure 9-(b), the load width was defined for the sandwiching plates. The load width is equal to the width of the sandwiching plate, and the load width of sandwiching plate is half the flange width in the reduced section. This compression stress is applied to half of the length of the steel plates.
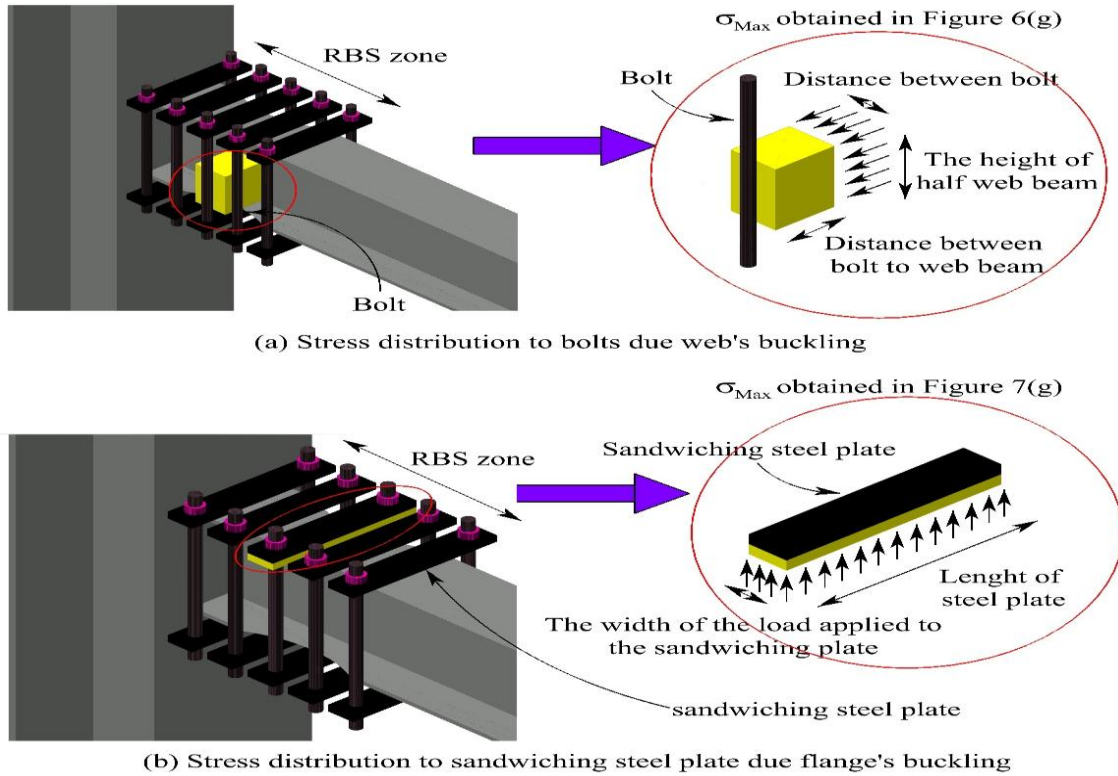
Fig 9. Pressure Distribution to the Bolts and Steel Plates in the Reduced Section Caused by Web and Flange Buckling

4. Design of Various Beam Sections

4.1. Design Process

In designing reduced beam section (RBS) following step should be conducted.

Step 1. Determining the Plastic Hinge Location
The main goal of considering the reduced section of the beams is to transfer the plastic joint from the beam flange-column weld area to the internal areas of the beam. For this purpose, the plastic moment of the beam is formed in the reduced sections. To determine the distance between the plastic hinge and the column, the limits must first be set for the a, b, and c values shown in Fig 10.

$$R = \text{Radius of cut} = \frac{4c^2 + b^2}{8c}$$

$$\begin{cases} 0.5b_{bf} \leq a \leq 0.75b_{bf} \\ 0.65d \leq b \leq 0.85d \\ 0.1b_{bf} \leq c \leq 0.25b_{bf} \end{cases}$$

Reduced beam section

a = horizontal distance from face of column flange

b = length of RBS cut

b_{bf} = width of beam flange

c = depth of cut at center of reduced beam section

d = depth of beam

Protected zone
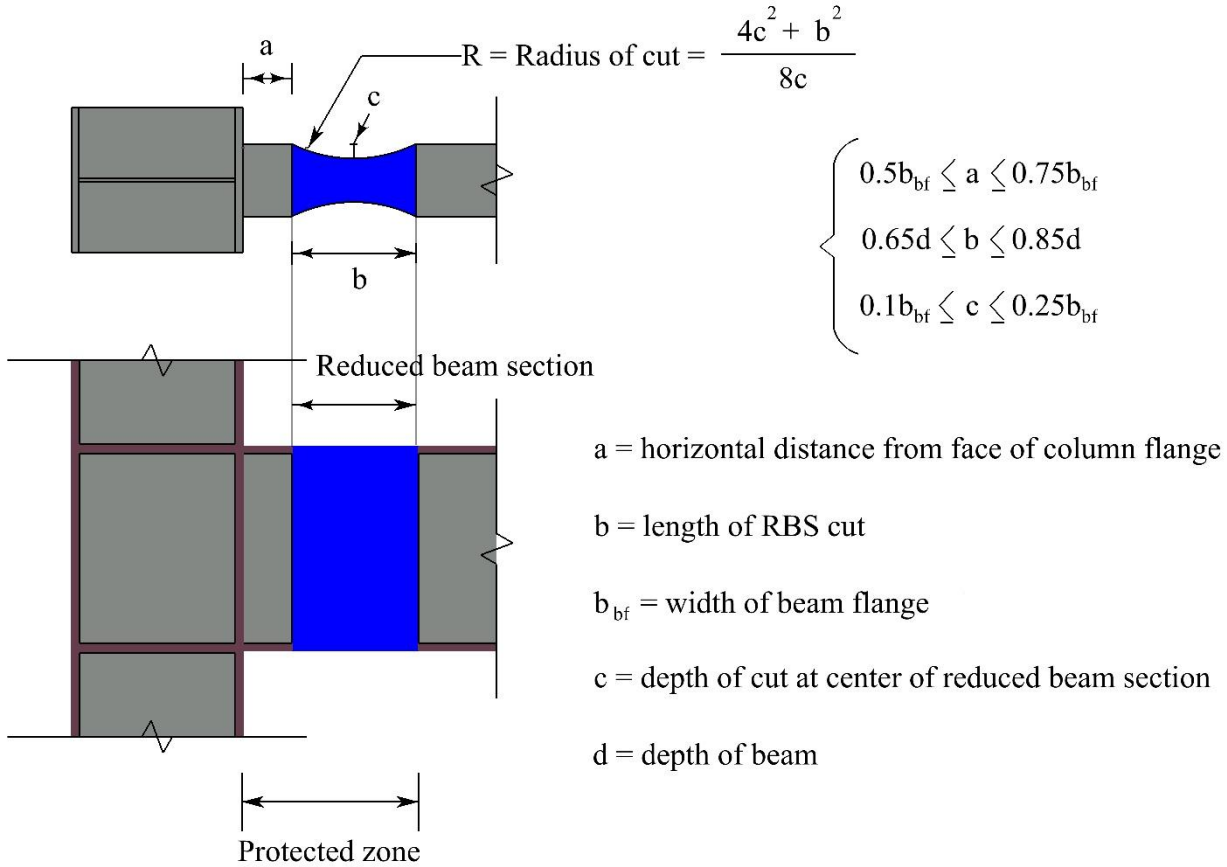
Fig 10. The Reduced Section of the RBS Beam

An initial approximation of these values can help determine the shear radius and location of the beam. For instance, the parameters a, b and c for the IPE300 are considered as 90mm, 230mm and 30mm, respectively. The middle of the cut curve is considered the exact location of the plastic joint. The distance of this location to the column is calculated as follows:

$$S_h = a + b/2 \qquad\qquad \text{Equation 1}$$

where, S_h is the distance of the beam–column connection to the reduced mid-section, which is 10.5 cm based on the parameters of the reduced section IPE300.

Step 2. Determining the Plastic Section Modulus for the Reduced Section of the Beam
The plastic section modulus at the center of the shear section is a function of the section's initial plastic modulus minus the separated section, which is written as follows in the AISC 358 [24] guidelines:

$$Z_e = Z_{xb} - 2ct_{bf}(d_b - t_{bf}) = Z_{RBS} \qquad \text{Equation 2}$$

Where, Z_{RBS}: the effective plastic modulus of a section (or connection) at the location of a plastic hinge (mm^3), Z_{xb}: the plastic section modulus of a beam (mm^3), c: the depth of cut at the center of the reduced beam section (mm), t_{bf}: the thickness of the beam flange (mm), (d_b): the beam's depth (mm). For instance, the defined parameters are Z_{RBS}=411.36 cm^3, c=30 mm, t_{bf} =10.7 mm, d_b =300mm, for the IPE300.

Step 3. Determining the Maximum Possible Flexural Moment in the Middle of the RBS
In this section, the maximum possible flexural moment (M_{pr}) in the reduced section will be determined. Based on the guideline equation, this moment is obtained as follows:

$$M_{pr} = C_{pr}R_yf_yZ_e \qquad\qquad \text{Equation 3}$$

where, based on yield stress (f_y) and the ultimate limit stress of steel (f_u), (R_y) the ratio of the expected yield

12

stress to the specified minimum yield stress and the C_{pr} value is obtained from Equation 4. According to Z_e, the plastic moment in the central area of the reduced section of beam is $M_{pr} = 142.16$ kN.m for IPE300, regarding $C_{pr} = 1.15$, $R_y = 1.1$, M_{pr} is Probable maximum moment at plastic hinge. The C_{pr} coefficient is the estimation of the increased connection strength that could arise due to phenomena such as strain hardening, partial confinement, or extra resistance. According to the AISC 358 [24] guidelines, this coefficient is obtained as follows:

$$C_{pr} = \frac{f_y + f_u}{2fy} \le 1.2 \qquad \text{Equation 4}$$

where, f_y is the yield stress of steel and f_u is the ultimate stress of steel.

Step 4. Determining the Shear Force in Middle of Each Reduced Section

In the following equation that obtains the shear force in the center of the reduced section, V_{RBS} is the shear force in the central section and V_{pr} is shear in the state where the reduced section has reached its maximum flexural capacity of M_{pr}.and V_{LL} Beam shear force at the center of the RBS caused by live load and V_{DL} is Beam shear force at the center of the RBS caused by dead load.

$$V_{RBS} = 1.2\ V_{DL} + V_{pr} + 0.5V_{LL} \qquad \text{Equation 5}$$

Step 5. Determining the Maximum Flexural Moment in the Column

In this stage, the flexural moment created in the column is calculated as follows:

$$M_{f =} M_{pr +} V_{RBS}S_h \qquad \text{Equation 6}$$

In Equation 6, the flexural moment in the beam–column connection is obtained in accordance with the shear in the reduced section of the RBS beam, M_f is maximum moment expected at face of column, which is $M_f = 142.876$ kN.m for reduced IPE300. In most cases considered for RBS beams, the flexural moment caused by widespread load between the connection and the reduced section is ignored.

Step 6. Calculating the Expected Plastic Flexural Moment for the Full Beam Section

In this stage, the maximum expected flexural capacity for the section will be obtained. This capacity is obtained from Equation 7:

$$M_{pe} = Z_{xb}R_{yb}f_{yb} \qquad \text{Equation 7}$$

According to Equation 7, the maximum flexural capacity is obtained by substituting the plastic modulus and yield stress, which is $M_{pe} = 173.3$ kN.m.

Step 7. Equation Control

In this stage, the maximum moment applied to the column must be compared with the beam's maximum flexural capacity. If the maximum moment applied to the column is greater than the flexural capacity, other values must be selected as the geometry of the reduced section. This is a trial and error process to ensure that the maximum moment is lower than the maximum capacity of the beam. The maximum beam capacity carries the φ_d coefficient.

$$(M_f/(\varphi_d\ M_{pe})) \le 1.0 \qquad \text{Equation 8}$$

$M_f = 142,876$ kN.m, $\varphi_d = 1$, and the beam's maximum flexural capacity of $M_{pe} = 173.3$ kN.m is obtained from Equation 7. Furthermore, the substitution of these values satisfies Equation 8.

4.2. Failure Mechanisms Considered Sections

In this study, based on variations in the dimensions of the reduced section of the RBS beam for various IPEs, which also changes the dimensions of the sandwiching plate and grout, various bolt sizes are checked for each section to obtain the best size for various beam sections. Regarding the procedure described in section to calculate the pressure applied to the bolts, plates were designed in the software with half the beam web dimensions for each IPE. The out-of-plane pressure created in this plate during buckling is applied to half the height of bolts based on their distance. The grout and sandwiching plate change based on the lengthening of the reduced section and the different widths of the beam web and flange in various IPEs. This ratio is based on the tested IPE300 dimensions. The load width applied to the bolts changes based on the distance of bolts. The load width applied to the bolts is defined in accordance with the distance of bolts. The load length is equal to the length of bolts. According to Figure 11-(a), during buckling in the reduced section of the beam, half the web was subjected to compressive stress while the other half experiences tensile stress. Moreover, the load width applied to the plates changes based on changes to the sandwiching plate and is half the length of the sandwiching plates. According to Figure 11-(b), during flange buckling at the reduced beam section, half the flange was subjected to pressure and the other half experiences tension.

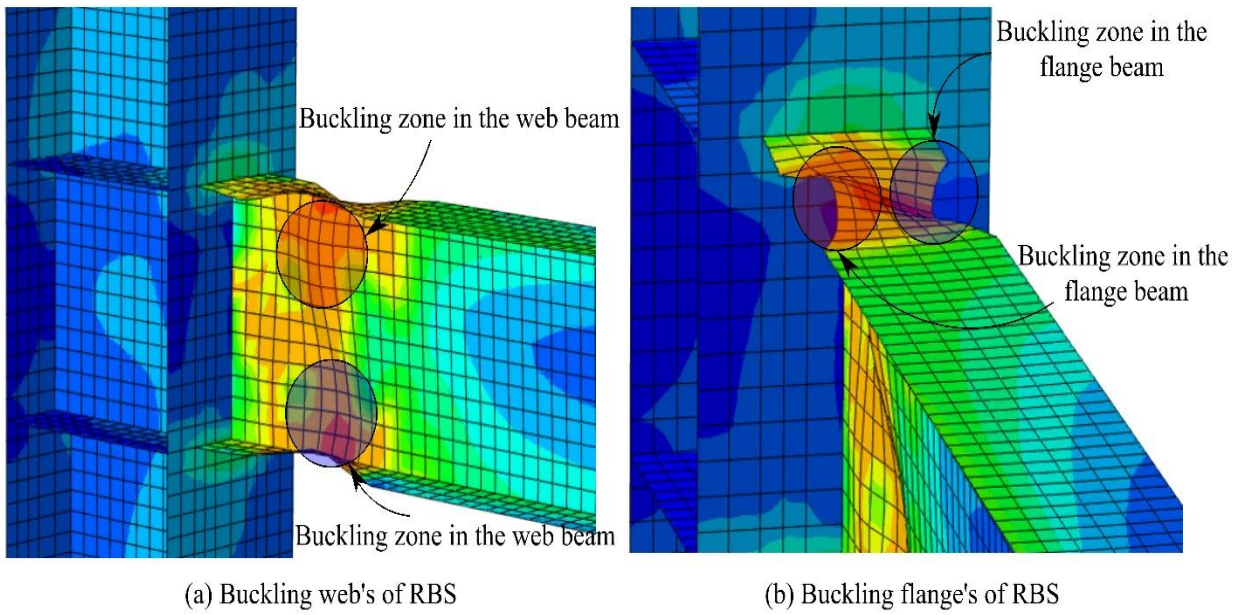(a) Buckling web's of RBS

(b) Buckling flange's of RBS

Fig 11. Pressure and Tensions Zones During the Buckling of the RBS Beam (IPE300)

To select the best size of bolts and sandwiching plates for each beam section, pressure was calculated based on the load surface of bolts and the sandwiching plate. Changing the size of the sandwiching plates and grout also changes the distance between bolts. Figure 12 demonstrates different dimensions of grout and sandwiching plate for the various sections analyzed by Zaferani *et al*, [23].
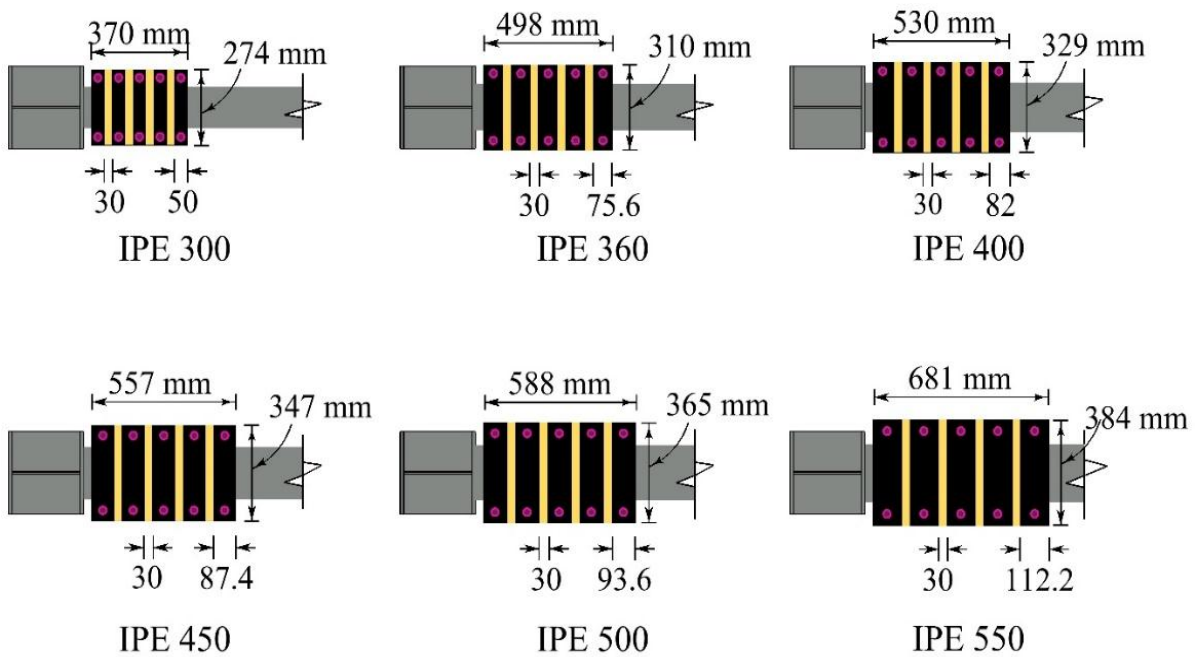
Fig 12.The Dimensions of Grout and Sandwiching Plate in Various Beam Sections

4.3. Analysis and Design of Bolts

The samples were modeled in ABAQUS. The 3D extrusion shell element was used for modeling the beam and column in software. The beam length is 2 m and the column length is 2.5 m. Table 1 defines the elastic and plastic properties of steel. The selected type of analysis is dynamic implicit. The support condition on both free sides of the column was defined as pinned. The reference points are placed in the bottom part of the column flange and the degrees of freedom of the other points on the two sides of the column's bottom flange are bound to the reference points. The pinned supports are placed in these two reference points. A reference point is defined in the free section of the beam to which the other points of the free surface are bounded. The load is applied to this reference point. The AISC 358 [24] loading protocol was used for loading the open side of the team. According to the steps described in Figure 6 and 7, the maximum strain has been obtained from FEM analyses' results of the reduced web and flange of the RBS beam. Figure 9 shows how to model beams and columns in finite element software.
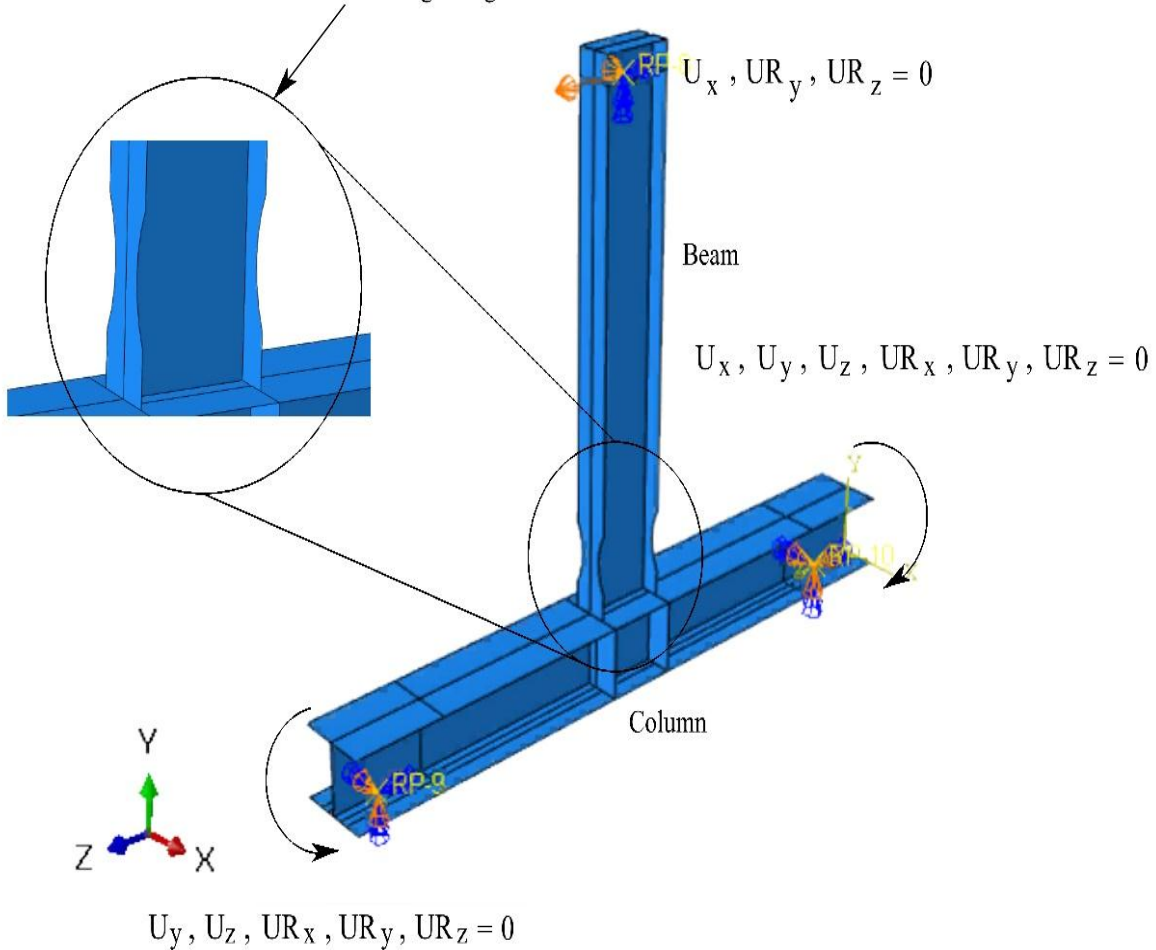
Fig 13. Node Binding Conditions in the RBS Models

The bolt was modeled with a solid extrusion element, and the elastic and plastic properties were applied to the model in accordance with table 1.

Table 1
The Properties of Materials

Component	Elasticity Modulus (GPa)	Yield Stress/cylinder strength (MPa)	Ultimate Stress (MPa)
Beam	202	432	553
Column	202	420	548
Strips	200	360	440
Bolt	210	400	510.8

Bolts with 10, 20, and 30 mm diameters were modeled for IPE300. The maximum out-of-plane stress for the modeled plane for half the web dimensions in IPE300 is 200 MPa. The maximum displacement and Von-Mises stress for these bolts is calculated along the external stress. The bolt with 10 mm diameter reached yield stress and the maximum Von-Mises stress of 408.4 MPa. The maximum displacement of the bolt with the diameter of 20 is 0.6 mm and its maximum Von-Mises stress in the deformed area reached 67.4 MPa. The bolt with 30 mm diameter had a maximum displacement of 0.1 mm and a maximum Von-Mises stress of 46.7 MPa. Then, the modeling process was repeated for IPE360, IPE400, IPE450, IPE500, and IPE550. Figure 14 shows the deformation of the bolts modeled in software for various cross sections. Figure 15 presents the maximum bolt displacement results for beams with various sections. Moreover, Figure 16 indicates the maximum Von-Mises tension in the part of the bolts with the greatest deformation for various sections of the beam. Bolts with 20 and 30 mm diameters were modeled for IPE360. The maximum out-of-plane stress in the modeled plate for half the dimensions of the web in IPE360 was 268.75 MPa, which was the stress applied to the bolts. The maximum displacement and Von Mises stress was calculated for the deformed section of these bolts, which remain in the elastic range. The bolt with 20 mm diameter reaches a maximum Von- Mises stress of 102.2 MPa and displacement of 1.2 mm and the

bolt with 30 mm diameter reaches a maximum Von-Mises stress of 76.1 MPa and displacement of 0.22 mm. The maximum out-of-plane stress in the modeled plate for the web dimensions of IPE400 was 286.25 MPa. The bolt with 20 mm diameter reaches a maximum Von-Mises stress of 119.6 MPa and displacement of 1.4 mm and the bolt with 30 mm diameter reached a maximum Von-Mises stress of 79.7 MPa and displacement of 0.2 mm. The maximum out-of-plane stress in the modeled plate with the web dimensions of IPE450 was 300.5 MPa, which remains in the elastic range. The bolt with 20 mm diameter reached a maximum Von-Mises stress of 139.6 MPa, and displacement of 1.8 mm and the bolt with 30 mm diameter reached a maximum Von-Mises stress of 84.6 MPa and displacement of 0.2 mm. The maximum out-of-plane stress for the modeled plate with the IPE500 dimensions was 317.5 MPa, a value in which the 20 mm diameter bolt reaches the yield boundary and maximum Von-Mises stress of 400 MPa and displacement of 3.1 mm. The bolt with 30 mm diameter reached the maximum Von Mises stress of 99.5 MPa and displacement of 0.2 mm. The maximum out-of-plane stress for the modeled plate for the web dimensions of IPE500 was 368.125 MPa. Under this stress, the bolt with 20 mm diameter reached yield stress. This bolt reached a maximum stress of 402 MPa and displacement of 11.4 mm, whereas the bolt with 30 mm diameter reached a maximum stress of 111.3 MPa and displacement of 0.3 mm.

For different IPE according to Fig. 6, the maximum stress was calculated and applied to the bolts.
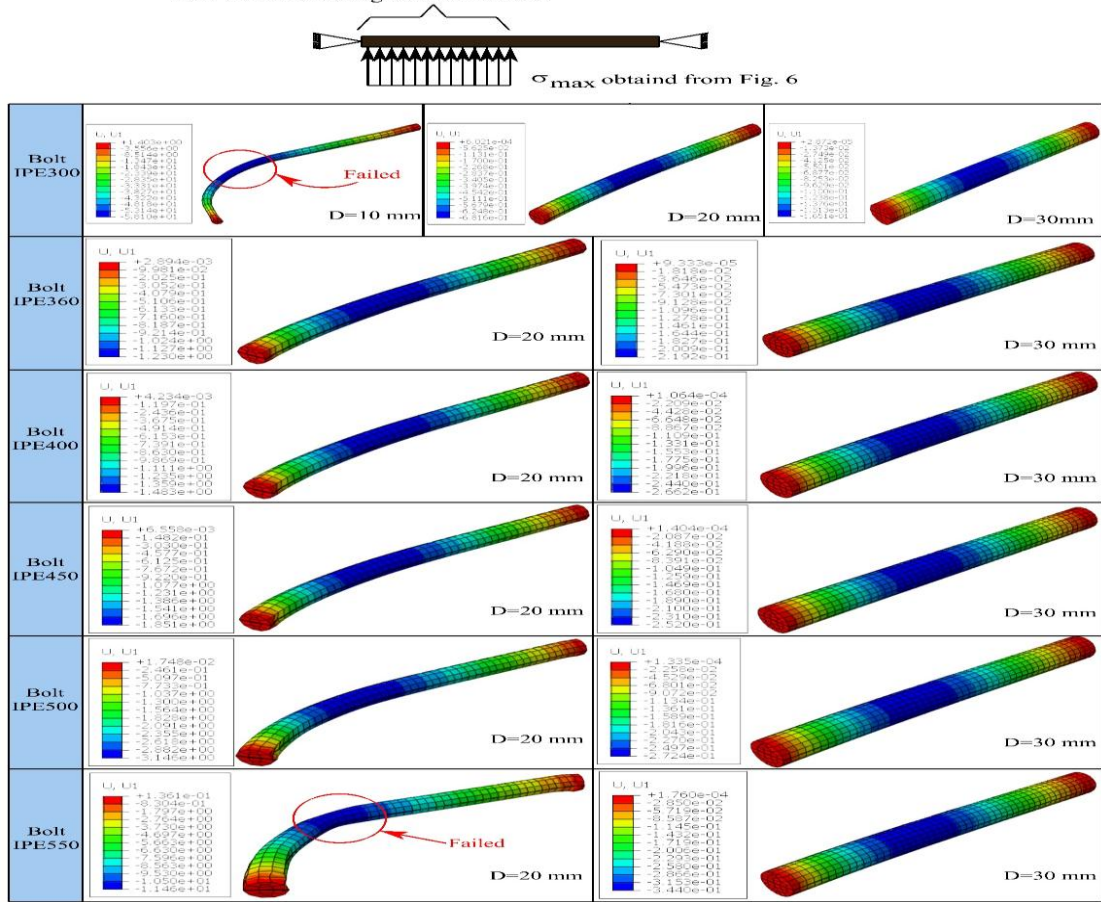Half bolt at buckling zone of the web

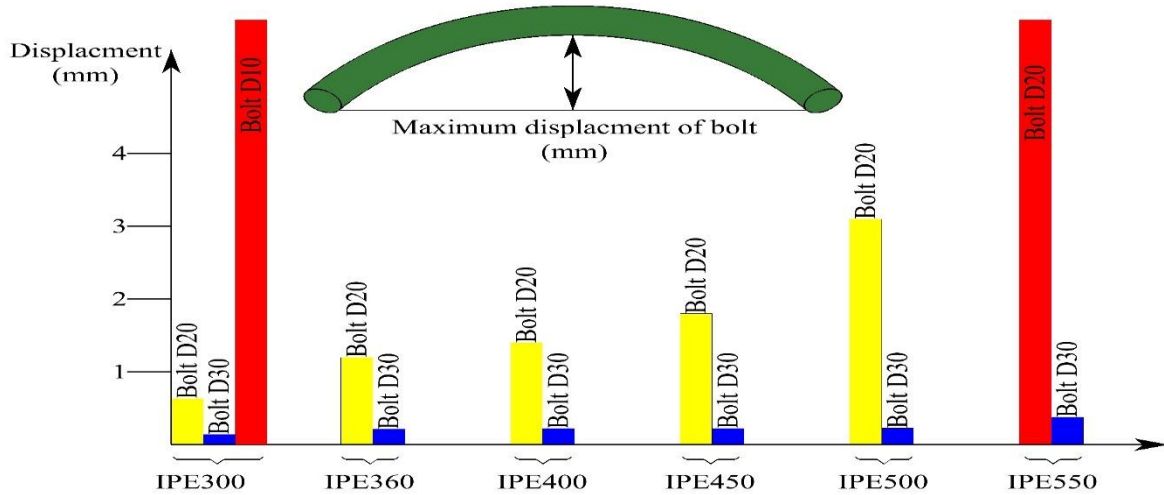Fig 14. The Displacement of Bolts Modeled for Various Sections of the Beam

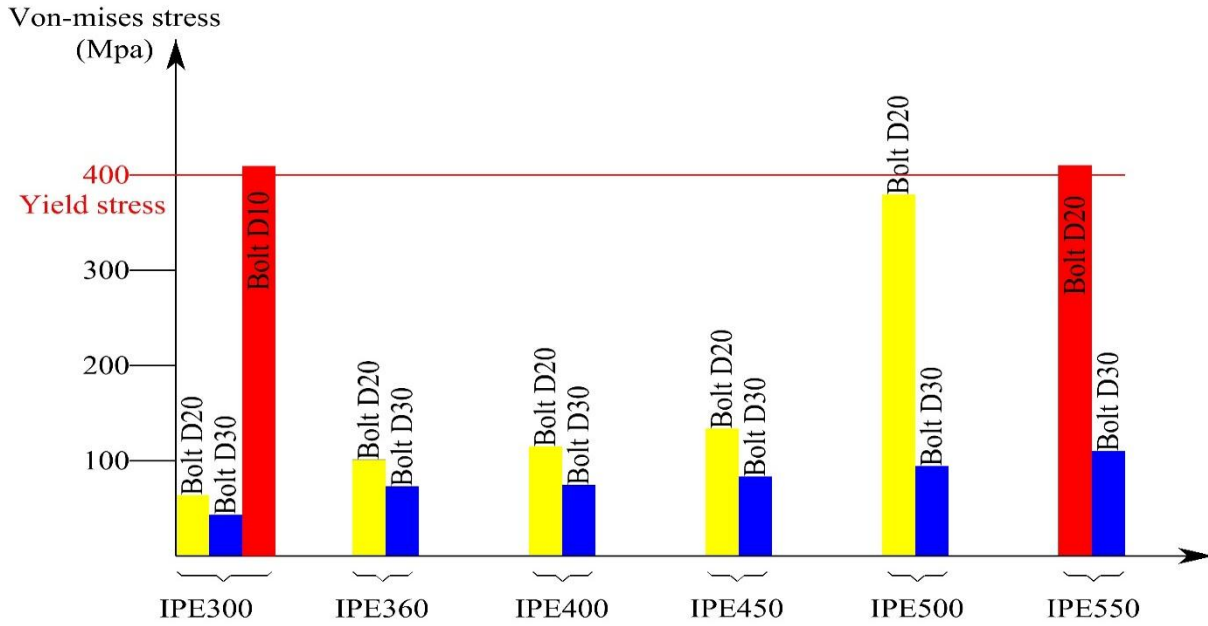Fig 15. The Displacement of Bolts for Various Sections

Fig 16. The Von-Mises Stress in Deformed Bolt for Various Sections

As illustrated in Fig 17, Steel plates with 10 and 20 mm thicknesses were modeled for IPE300. The maximum out-of-plane stress in the plate modeled for the reduced flange section is 1.5 MPa in IPE300. The maximum displacement and stress was calculated for the deformed section of these steel plates. The steel plate with 10 mm thickness reaches a maximum stress of 99.9 MPa and displacement of 0.8 mm. The maximum displacement of the steel plate with 20 mm thickness reaches 0.1, and the maximum Von-Mises stress in the deformed section reached 26.6 MPa. Then, the modeling process was repeated for IPE360, IPE400, IPE450, IPE500, and IPE550. Figure 17 shows the deformation of the sandwiching plate modeled in software for various cross sections. Figure 18 shows the maximum displacement of these plates for various sections. In addition, Figure 19 shows the maximum Von-Mises stress in the part of the plates with the greatest deformation for various sections of the beam. Steel plates with 10 and 20 mm thicknesses were modeled for IPE3360. The plate with 10 mm thickness reaches a maximum Von-Mises stress of 119.8 MPa and displacement of 1.3 mm and the plate with 20 mm thickness reached a maximum Von Mises stress of 36.6 MPa and displacement of 0.15 mm. For IPE400, the steel plate with 10 mm thickness reached a maximum stress of 131 MPa and displacement of 1.7 mm and the plate with 20 mm thickness reached a maximum Von-Mises stress of 36.8 MPa and displacement of 0.2 mm. For IPE450, the steel plate with 10 mm thickness reaches a maximum stress of 143.9 MPa and displacement of 2.2 mm and the steel plate with 20 mm thickness reached a maximum Von-Mises stress of 40.9 MPa and displacement of 0.28 mm. For IPE500, the steel plate with 10 mm thickness reached a maximum stress of 170.3 MPa and displacement of 2.8 mm and the steel plate with 20 mm thickness reaches a maximum Von-Mises stress of 45.1 MPa and displacement of 0.34 mm. For IPE550, the steel plate with 10 mm thickness reached a maximum stress of 186.5 MPa and displacement of 6.3 mm, and the sandwiching plate with 20 mm thickness reached a maximum Von-Mises stress of 49.2 MPa and displacement of 0.4 mm.

For different IPE according to Fig. 7, the maximum stress was calculated and applied to the sandwiching steel strip.

Half of sandwiching steel strip
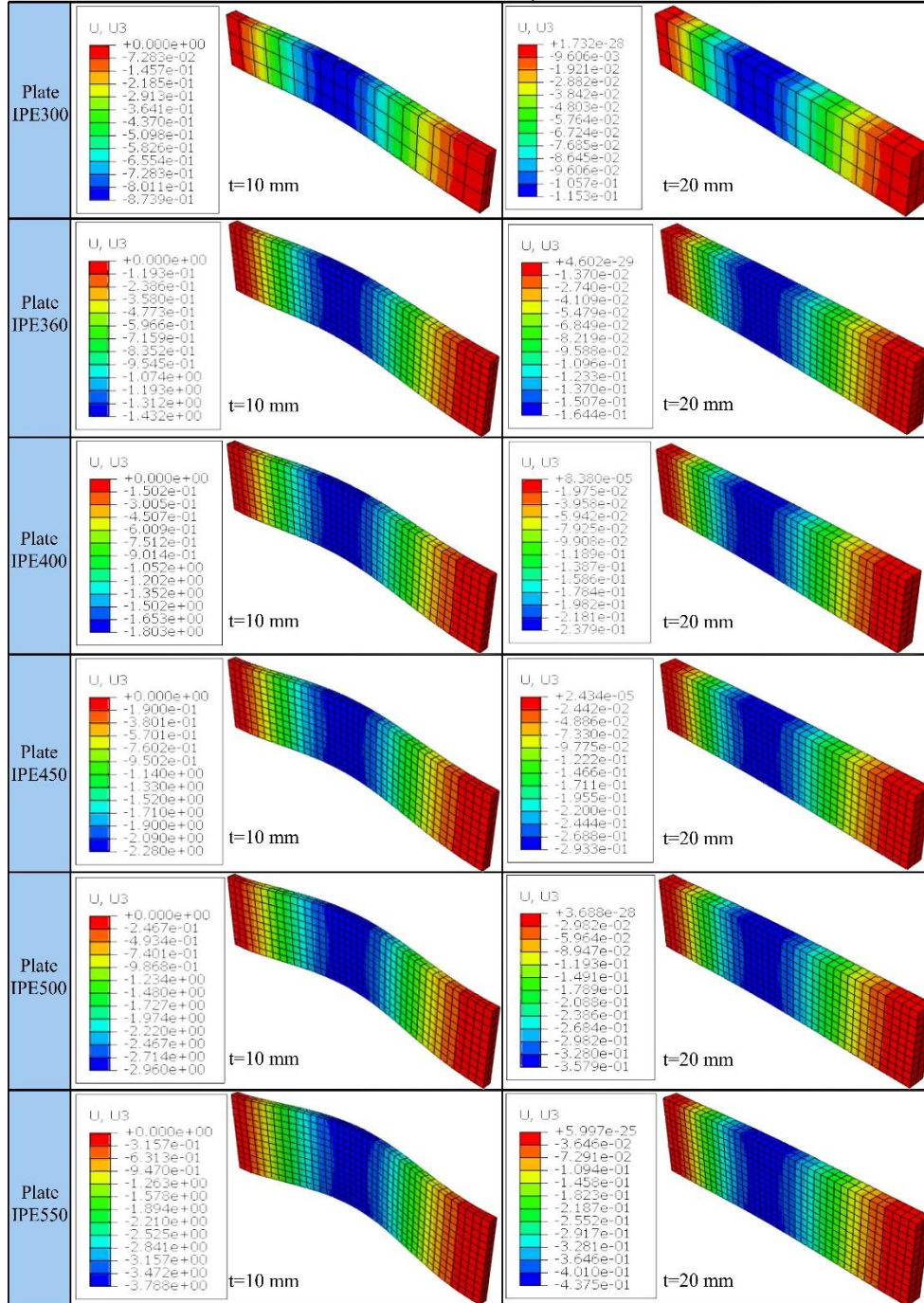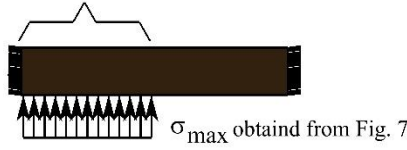
σ_{max} obtaind from Fig. 7

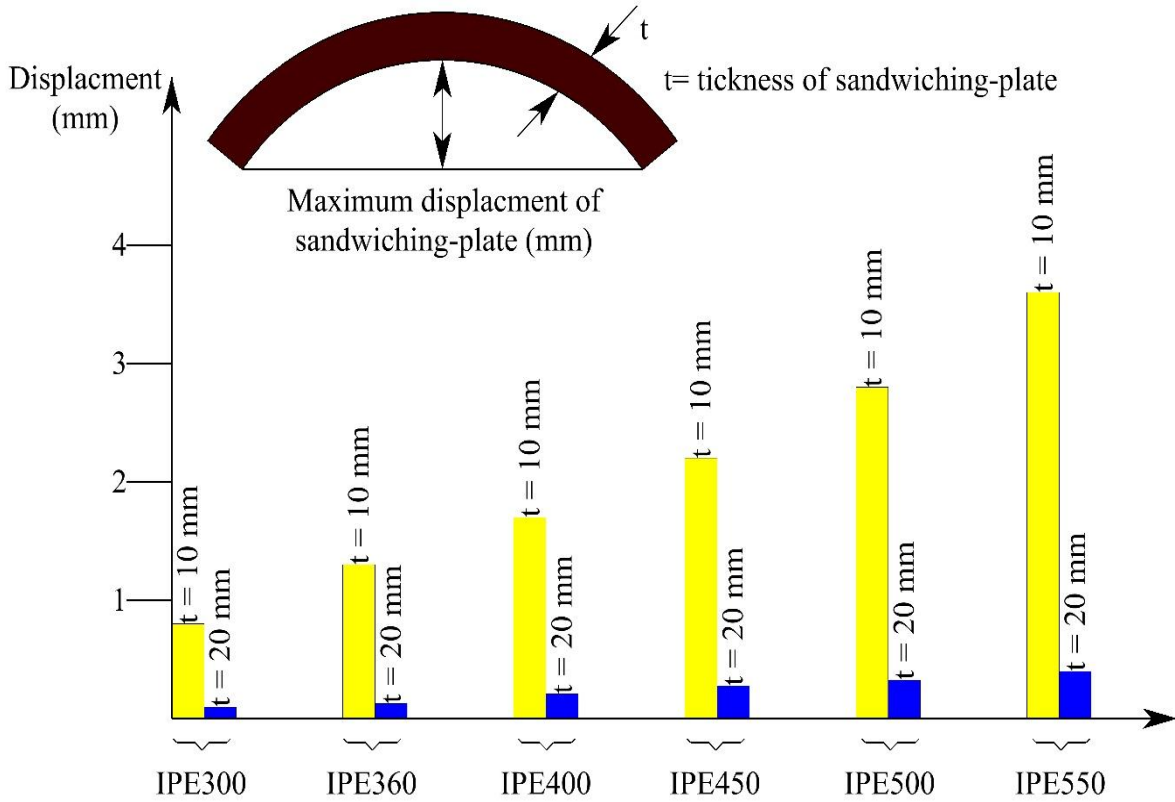Fig 17. Deformation of the Sandwiching Plates Modeled for Various Sections of the Beam

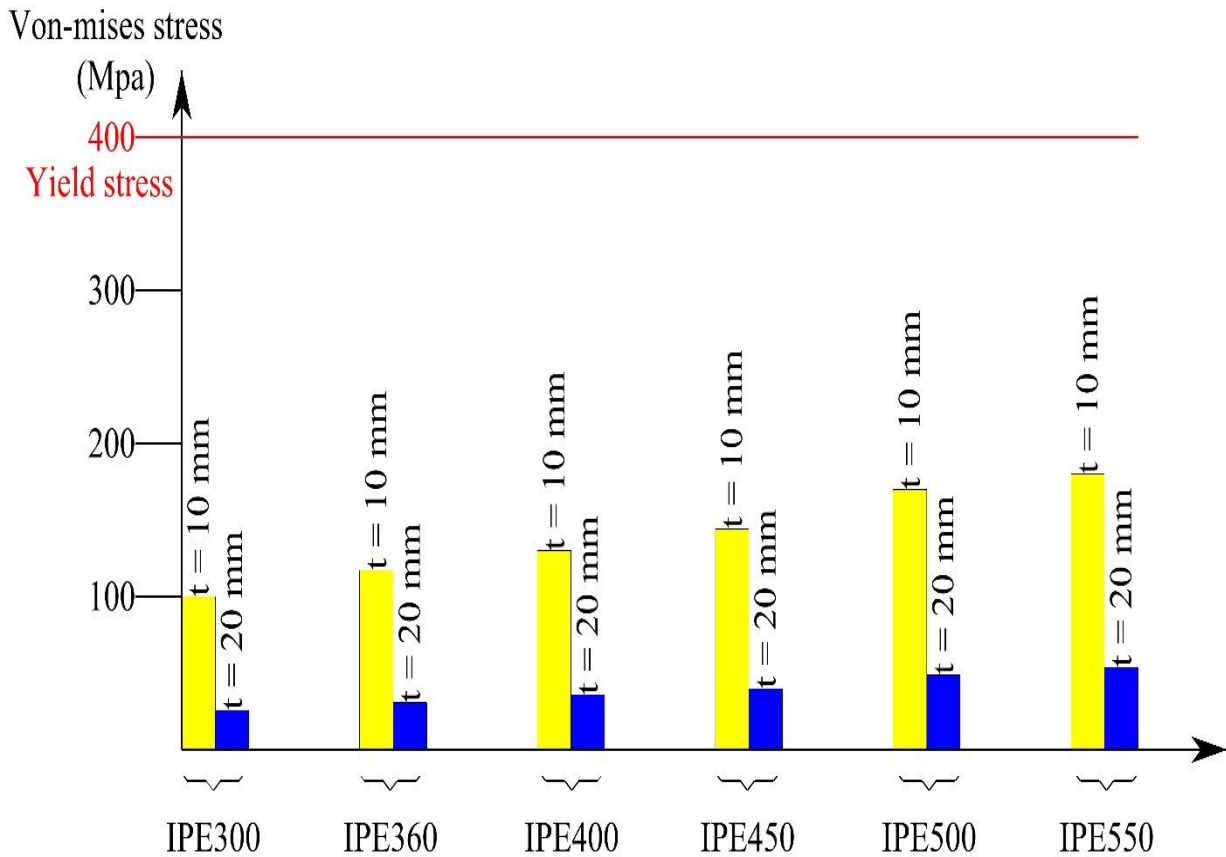Fig 18. Displacement of Sandwiching Plates for Various Sections

Fig 19. The Von-Mises Stress in Sandwiching Plate Deformations for Various Sections

5. Conclusion

The Proposed HS–RBS system consists of grout, bolts, and steel plates. It prevents local buckling in the reduced section of the RBS beam. This study proposed a simplified design method for the diameter of bolts and the thickness of sandwiching plates using FEM. This method determines bolt diameter and sandwiching plate thickness for various sections of HS–RBS beams. To calculate the diameter of bolts in the software, the strain along the beam was first measured in the reduced section. Then, a plate with half the dimensions of the reduced section of the beam web was modeled in software and was subjected to longitudinal displacement to reach target maximum

strain. Out of plate stress was measured when the critical element reached a strain equal to the maximum strain along the longitudinal axis of the beam. Then, obtained stress was applied to bolts with various diameters to obtain the displacement and Von-Mises stress in bolts. The sizes of bolts with 10, 20, and 30 mm diameters were compared for the HS–RBS system. The maximum displacement of bolts and Von-Mises stress in the deformed section of the models were then compared to determine the best bolt size for each section. Moreover, sandwiching plates with 10 and 20 mm thicknesses were compared in each section of the beams.

References

[1]   FEMA, F., *350—Recommended seismic design criteria for new steel moment-resisting frames.* Washington (DC): Federal Emergency Management Agency, 2000.

[2]   Plumier, A. *New idea for safe structures in seismic zones.* in *IABSE Symposium-Mixed Structures Including New Materials.* 1990.

[3]   Popov, E.P., T.-S. Yang, and S.-P. Chang, *Design of steel MRF connections before and after 1994 Northridge earthquake.* Engineering Structures, 1998. 20(12): p. 1030-1038.

[4]   Plumier, A., *Behaviour of connections.* Journal of Constructional Steel Research, 1994. 29(1-3): p. 95-119.

[5]   M.D. Engelhardt, T. Winneberger, A.J. Zekany, T.J. Potyraj, *The dogbone connection: Part II.* Modern Steel Construction, 1996. 36(8): p. 46-55.

[6]   MD. Engelhardt, GT. Fry,S. Jones,M. Venti, S. Holiday, *Behavior and design of radius cut reduced beam section connections.* A draft report of SAC task, 2000. 7.

[7]   FEMA 351, *Recommended Seismic Evaluation and Upgrade Criteria for Existing Welded Steel Moment-frame Buildings.* Vol. 351. 2000: Federal Emergency Management Agency.

[8]   Roeder, C.W., *Connection performance for seismic design of steel moment frames.* Journal of Structural Engineering, 2002. 128(4): p. 517-525.

[9]   Cheol-Ho Lee, Sang-Woo Jeon, Jin-Ho Kim, Chia-Ming Uang., *Effects of panel zone strength and beam web connection method on seismic performance of reduced beam section steel moment connections.* Journal of Structural Engineering, 2005. 131(12): p. 1854-18.65

[10] Hedayat, A.A. and M. Celikag, *Post-Northridge connection with modified beam end configuration to enhance strength and ductility.* Journal of Constructional Steel Research, 2009. 65(7): p. 1413-1430.

[11] Lignos, D.G., D. Kolios, and E. Miranda, *Fragility assessment of reduced beam section moment connections.* Journal of Structural engineering, 2010. 136(9): p. 1140-1150.

[12] Mirghaderi, S.R., S. Torabian, and A. Imanpour, *Seismic performance of the Accordion-Web RBS connection.* Journal of Constructional Steel Research, 2010. 66(2): p. 277-288.

[13] Deylami, A. and A.M. Tabar, *Promotion of cyclic behavior of reduced beam section connections restraining beam web to local buckling.* Thin-Walled Structures, 2013. 73: p. 112-120.

[14] Atashzaban A, Hajirasouliha I, Jazany RA,Izadinia, *Optimum drilled flange moment resisting connections for seismic regions.* Journal of Constructional Steel Research, 2015. 112: p. 325-338.

[15] Morshedi, M.A., K.M. Dolatshahi, and S. Maleki, *Double reduced beam section connection.* Journal of Constructional Steel Research, 2017. 138: p. 283-297.

[16] Shin, M., Kim, S., *Seismic toughness and failure mechanisms of reduced web-section beams: Phase 1 tests.* Engineering Structures, 2017. 141: p. 198-216.

[17] Fanaie, N. and H.S. Moghadam, *Experimental study of rigid connection of drilled beam to CFT column with external stiffeners.* Journal of Constructional Steel Research, 2019. 153: p. 209-221.

[18] Mohammad Davarpanah, Hamid Ronagh, Parham Memarzadeh, Farhad Behnamfar, *Cyclic behavior of welded elliptical-shaped RWS moment frame.*

Journal of Constructional Steel Research, 2020. 175: p. 106319.

[19] Nazaralizadeh, H, Hamid Reza Ronagh, Parham Memarzadeh, Farhad Behnamfar, *A practical design approach to bolted end-plate vertical-slits RWS connection.* Bulletin of Earthquake Engineering, 20 :(1)20 .22p. 547-586.

[20] Liu, C., J. Wu, and L. Xie, *Seismic performance of buckling-restrained reduced beam section connection for steel frames.* Journal of Constructional Steel Research, 2021. 181: p. 106622.

[21] Bompa, D.V. and A.Y. Elghazouli. *Ultimate cyclic response of steel reduced beam section connections*. in *3rd European Conference on Earthquake Engineering & Seismology (3ECEES)*. 2022.

[22] Saberi, V.,Saberi, H.,Salimikia, M.,Sadeghi, A., *Investigation the cyclic behavior of rigid RBS connections with horizontal and vertical stiffeners in steel moment-resisting frame.* Amirkabir Journal of Civil Engineering, 2022. 54(4): p. 1273-1310.

[23] Alireza Zaferani, Pasha Javadi, Parham Memarzadeh, *A hybrid-sandwiching system for buckling-restraining of reduced beam sections.* Journal of Constructional Steel Research, 2023. 209: p. 108026.

[24] ANSI/AISC 358—16, *Prequalified Connections for Special and Intermediate Steel Moment Frames for Seismic Applications*, American Institute of Steel Construction, Chicago, 358-316.